A NEW ONE-SHOT POINTWISE SOURCE RECONSTRUCTION METHOD

T. J. MACHADO, J. S. ANGELO AND A. A. NOVOTNY

Abstract. In this work a new pointwise source reconstruction method is proposed. From a single pair of boundary measurements, we want to completely characterize the unknown set of pointwise sources, namely, the number of sources, their locations and intensities. The idea is to rewrite the inverse source problem as an optimization problem, where a Kohn-Vogelius type functional is minimized with respect to a set of admissible pointwise sources. The resulting second-order reconstruction algorithm is non-iterative and thus very robust with respect to noisy data. Finally, in order to show the effectiveness of the devised reconstruction algorithm, some numerical experiments into two spatial dimensions are presented.

1. Introduction

In this paper we deal with an inverse potential problem, which consists of reconstructing an unknown source located within an open domain $\mathcal{D}$ using information obtained on a subset Γ_m of $\partial\mathcal{D}$, where $\partial\mathcal{D}$ denotes the boundary of $\mathcal{D}$. Usually, it is assumed that the source to be recovered is given by a piecewise constant function with support contained in $\mathcal{D}$, namely

$$b(x) = \begin{cases} \alpha_1 & \text{if} \quad x \in \omega, \\ \alpha_2 & \text{if} \quad x \in \mathcal{D} \setminus \omega. \end{cases} \tag{1.1}$$

In this case, to reconstruct the unknown source means to determine the values $\alpha_1 \in \mathbb{R}$ and $\alpha_2 \in \mathbb{R}$ as well as the shape and the topology of the set ω. In [16] it was shown that the reconstruction is possible only if α_1 and α_2 are given and if ω is convex or star-shaped with respect to its barycenter. Important contributions in the solution of a wide class of inverse problems have relied on standard approaches based on level-set methods [21, 17] or asymptotic analysis [1, 9]. In particular, see for instance recent papers dealing with source reconstruction problem from total [6] and partial [7] boundary measurements, respectively, where ω is approximated by a number of ball shaped anomalies.

In contrast to the above mentioned papers, here we are interested in the reconstruction of pointwise sources. Formally, the effect of a ball in the boundary measurements is exactly the same as that of a pointwise source of same total mass. Therefore, in this paper we extend – from the mathematical point of view – the theory developed in [6, 7] by considering that the unknown source is given by a number of Dirac-mass, namely

$$b(x) = \sum_{i=1}^{m} \alpha_i \delta(x - x_i), \tag{1.2}$$

where m is the number of sources, α_i is the intensity and x_i the location of each source. The main advantage of recovering a set of concentrated sources is that it eliminates the concern regarding the shape of their support. On the other hand, along with the locations x_i, we must determine the number m and intensities α_i of the anomalies in order to completely characterize the unknown source b. In [2] it was proved that it is possible to reconstruct a source in the form (1.2) from a single pair of boundary measurements provided that $|\Gamma_m| \neq 0$. Among the possible applications for this kind of problem, we highlight:

- Location of pollution sources in a given environment [3, 16].
- Identification of monopoles and dipoles in electroencephalography and magnetoencephalography [13, 15].

Key words and phrases. pointwise source reconstruction; non-iterative second-order algorithm; Kohn-Vogelius criterion; sensitivity analysis.

- Detecting the epicenter of a given earthquake, knowing its effect on the earth's surface [20].
- Detection of hidden anomalies in the density of the earth, from measurement of the gravity field on its surface [4].

Since we are dealing with pointwise sources, standard approaches of resolution of inverse problems cannot be directly applied in this context. Therefore, in order to solve the inverse problem we are dealing with, it is rewritten as an optimization problem where a Kohn-Vogelius type functional [19] is minimized with respect to a set of admissible pointwise sources. The Kohn-Vogelius criterion measures a quadratic form of the misfit between the solutions of two auxiliary problems, one containing information on the boundary measurement and the other one containing information on the boundary excitation. Therefore, it vanishes over the solution of the inverse problem. The resulting second-order reconstruction algorithm is non-iterative and thus very robust with respect to noisy data. Finally, in order to show the effectiveness of the devised reconstruction algorithm, some numerical experiments into two spatial dimensions are presented.

The paper is organized as follows. In Section 2 the mathematical formulation of the inverse potential problem we are dealing with is introduced. In Section 3 the inverse problem is rewritten as an optimization problem. In Section 4 the Kohn-Vogelius functional is minimized with respect to a set of admissible pointwise sources and the resulting reconstruction algorithm is devised. Some numerical experiments of pointwise source reconstruction from total and partial boundary measurements are presented in Section 5. Finally, in Section 6 the paper ends with some concluding remarks.

2. Problem Formulation

Let $\mathcal{D} \subset \mathbb{R}^2$ be an open domain with Lipschitz boundary, denoted by $\partial\mathcal{D}$. Let Γ_m be a subset of $\partial\mathcal{D}$ with non-zero Lebesgue measure. The inverse source problem consists in determining the unknown source b^* from the Cauchy data u^* and q^* in the following elliptic boundary value problem:

$$\left\{ \begin{array}{rcl} -\Delta u &=& b^* \\ u &=& u^* \\ -\partial_n u &=& q^* \end{array} \right\} \begin{array}{ll} \text{in} & \mathcal{D}, \\ \text{on} & \Gamma_m. \end{array} \tag{2.1}$$

It is well-known that the above inverse source problem may have no unique solution. To recover uniqueness it is necessary to restrict the set in which b^* belongs. In this work, we consider the following set of admissible solutions:

$$C_\delta(\Omega) = \left\{ b : \Omega \to \mathbb{R}; b(x) = \sum_{i=1}^{n} \alpha_i \delta(x - x_i) \right\}, \tag{2.2}$$

where $n \in \mathbb{N}$, $\alpha_i \in \mathbb{R} \setminus \{-\infty, +\infty\}$ and $x_i \in \Omega$, with $i \in \{1, ..., n\}$. By assumption, the open and bounded subdomain $\Omega \subset \mathcal{D}$ contains the support of the unknown source b^*. Moreover, the distribution $\delta : \Omega \to \mathbb{R}$ is defined by:

$$\int_{\mathbb{R}^2} \delta(x - y)\varphi(y)\, dy = \varphi(x) \quad \forall \varphi \in C_c^\infty(\mathbb{R}^2; \mathbb{R}).$$

From the definition for the set of admissible solutions (2.2), the unknown source $b^* \in C_\delta(\Omega)$ can be represented as follows:

$$b^*(x) = \sum_{i=1}^{m^*} \alpha_i^* \delta(x - x_i^*). \tag{2.3}$$

Therefore, solving the inverse potential problem (2.1) in $C_\delta(\Omega)$ means to find m^*, α_i^* and x_i^*, which denote the number, intensities and locations of the unknown pointwise sources, respectively. In particular, we are going to address two distinct situations with respect to the domain $\mathcal{D}$, which are:

- Case 1: We suppose that $\mathcal{D}$ is a bounded domain in $\mathbb{R}^2$ and that Γ_m coincides with $\partial\mathcal{D}$, namely $\Gamma_m = \partial\mathcal{D}$. Therefore, total boundary measurement (u^*, q^*) on Γ_m is available. See sketch in Fig. 1(a).
- Case 2: We assume that $\mathcal{D}$ is the half-plane in $\mathbb{R}^2$ and that Γ_m is a subset of $\partial\mathcal{D}$, namely $\Gamma_m \subsetneq \partial\mathcal{D}$. Therefore, only partial boundary measurement (u^*, q^*) on Γ_m is available. See sketch in Fig. 1(b).

Since by assumption the domain Ω contains the support of the unknown source b^*, the inverse problem associated with each one of the above cases can be defined in Ω instead of $\mathcal{D}$. Let us denote the boundary of Ω by $\partial\Omega$. In the Case 1 we have $\Omega = \mathcal{D}$ and $\Gamma_m = \partial\Omega$. While in the Case 2, $\Gamma_m \subsetneq \partial\Omega$ and its complement is denoted by $\Gamma = \partial\Omega \setminus \Gamma_m$, where Γ is a fictitious boundary used in the reformulation of the inverse problem in the next section. See sketch in Fig. 1.

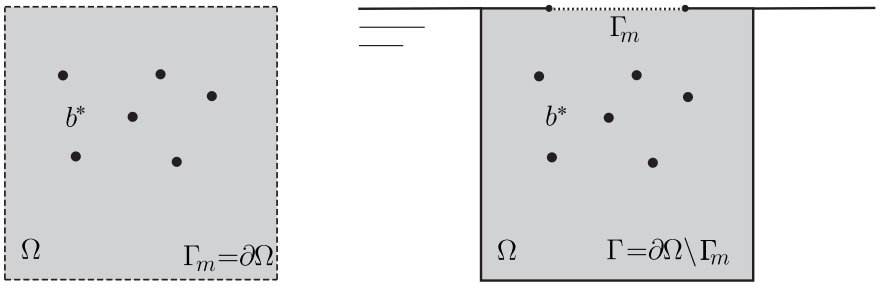

(a) Case 1: $\mathcal{D}$ is bounded (b) Case 2: $\mathcal{D}$ is unbounded

FIGURE 1. Problems setting.

3. Problem Reformulation

According to [2], the inverse potential problem (2.1) has a unique solution within the set $C_\delta(\Omega)$. However, stability of the reconstruction is still an issue mainly in the presence of noise. In order to overcome this difficulty, it is usual to introduce a regularization on the inverse operator, such as total variation techniques or Tikhonov regularization. In contrast to regularization strategies, in this paper we propose to rewrite the inverse problem we are dealing with as an optimization problem where a Kohn-Vogelius type functional is minimized with respect to the set of admissible pointwise sources $C_\delta(\Omega)$ defined in (2.2).

In order to define the optimization problem, let us introduce the following functional based on the Kohn-Vogelius criterion [19]:

$$\mathcal{J}(u^D, u^N) = \int_\Omega (u^D - u^N)^2 \, dx. \tag{3.1}$$

The functions u^D and u^N are solutions of two direct auxiliary problems depending on the pointwise source $b \in C_\delta(\Omega)$. One of them is associated to the Dirichlet data u^* whereas the other one contains information on the Neumann data q^*. These auxiliary problems are constructed in such a way that the Kohn-Vogelius functional (3.1) attains its minimum value over the solution of the inverse problem (2.1). In Sections 3.1 and 3.2 the auxiliary problems respectively related to Cases 1 and 2 are presented. We note that since the auxiliary problems depend on $b \in C_\delta(\Omega)$, then minimizing (3.1) with respect to the set of admissible pointwise sources $C_\delta(\Omega)$ can be seen as an optimal control problem in measure space, widely studied in the literature. See, for instance, [5, 8, 10, 22].

3.1. Auxiliary Problems: Case 1.

In the Case 1, the Cauchy data is available on the whole boundary $\partial\Omega$. Therefore, the auxiliary problems related to this case are given by:

$$\begin{cases} -\Delta u^D = b & \text{in } \Omega, \\ u^D = u^* & \text{on } \partial\Omega. \end{cases} \tag{3.2}$$

and

$$\left\{\begin{array}{rcll} -\Delta u^N &=& b+c & \text{in} \quad \Omega, \\ -\partial_n u^N &=& q^* & \text{on} \quad \partial\Omega, \\ \displaystyle\int_\Omega u^N\,dx &=& \displaystyle\int_\Omega u^D\,dx, & \end{array}\right. \tag{3.3}$$

where $b \in C_\delta(\Omega)$ is a given source, representing an initial guess. In addition, the compatibility constant c is given by

$$c = \frac{1}{|\Omega|}\left(\int_{\partial\Omega} q^*\,dS - \int_\Omega b\,dx\right), \tag{3.4}$$

where $|\Omega|$ is the Lebesgue measure of the set Ω.

3.2. **Auxiliary Problems: Case 2.** Let us consider Case 2, where the data u^* and q^* are known only on a part of $\partial\Omega$, namely Γ_m. Therefore, we have to complement the information on the remainder boundary Γ. See Fig. 1(b). The idea is to introduce the Newtonian potential

$$u^T[b](x) = -\int_{\mathbb{R}^2} \frac{1}{2\pi}\log\|x-y\|b(y)\,dy, \quad \forall x \in \mathbb{R}^2. \tag{3.5}$$

Then, the auxiliary problems are defined as follows:

$$\left\{\begin{array}{rcll} -\Delta u^D &=& b & \text{in} \quad \Omega, \\ u^D &=& u^* & \text{on} \quad \Gamma_m, \\ u^D &=& u^T[b] & \text{on} \quad \Gamma \end{array}\right. \tag{3.6}$$

and

$$\left\{\begin{array}{rcll} -\Delta u^N &=& b & \text{in} \quad \Omega, \\ -\partial_n u^N &=& q^* & \text{on} \quad \Gamma_m, \\ u^N &=& u^T[b] & \text{on} \quad \Gamma, \end{array}\right. \tag{3.7}$$

where $b \in C_\delta(\Omega)$ is a given source.

4. Sensitivity Analysis

Let us minimize the Kohn-Vogelius functional (3.1) with respect to the set of admissible solutions (2.2). Therefore, the idea is to perturb the source b by introducing a number m of pointwise sources with arbitrary locations and intensities. The perturbed source $b_\delta \in C_\delta(\Omega)$ is defined as follows

$$b_\delta(x) = b(x) + \sum_{i=1}^m \alpha_i \delta(x - x_i). \tag{4.1}$$

Associated with the perturbed source b_δ there are two new perturbed boundary value problems, whose solutions are denoted by u_δ^D and u_δ^N. The auxiliary problems related to Cases 1 and 2 are presented in Sections 4.1 and 4.2, respectively. The perturbed counterpart of the Kohn-Vogelius functional is given by

$$\mathcal{J}(u_\delta^D, u_\delta^N) = \frac{1}{2}\int_\Omega (u_\delta^D - u_\delta^N)^2\,dx. \tag{4.2}$$

After subtracting the original (3.1) from the perturbed (4.2) Kohn-Vogelius functional, we obtain

$$\begin{aligned} \mathcal{J}(u_\delta^D, u_\delta^N) - \mathcal{J}(u^D, u^N) &= \frac{1}{2}\int_\Omega \left[(u_\delta^D - u_\delta^N)^2 - (u^D - u^N)^2\right]\,dx \\ &= \frac{1}{2}\int_\Omega \left[(u_\delta^D + u^D) - (u_\delta^N + u^N)\right]\left[(u_\delta^D - u^D) - (u_\delta^N - u^N)\right]\,dx\,. \end{aligned} \tag{4.3}$$

Now, we introduce the following ansätze for u_δ^D and u_δ^N

$$u_\delta^D - u^D = \sum_{i=1}^m \alpha_i v_i \quad \Rightarrow \quad u_\delta^D + u^D = \sum_{i=1}^m \alpha_i v_i + 2u^D\,, \tag{4.4}$$

and

$$u_\delta^N - u^N = \sum_{i=1}^m \alpha_i (v_i + h_i) \quad \Rightarrow \quad u_\delta^N + u^N = \sum_{i=1}^m \alpha_i (v_i + h_i) + 2u^N \, . \tag{4.5}$$

Finally, the corresponding boundary value problems to the functions v_i and h_i are presented in Sections 4.1 and 4.2, respectively associated with Cases 1 and 2.

4.1. **Perturbed Problems: Case 1.** The perturbed counterparts of problems (3.2) and (3.3) associated with complete boundary measurement are written as:

$$\left\{ \begin{array}{rcl} -\Delta u_\delta^D &=& b_\delta \quad \text{in} \quad \Omega, \\ u_\delta^D &=& u^* \quad \text{on} \quad \partial\Omega \end{array} \right. \tag{4.6}$$

and

$$\left\{ \begin{array}{rcll} -\Delta u_\delta^N &=& b_\delta + c_\delta & \text{in} \quad \Omega, \\ -\partial_n u_\delta^N &=& q^* & \text{on} \quad \partial\Omega, \\ \displaystyle\int_\Omega u_\delta^N \, dx &=& \displaystyle\int_\Omega u_\delta^D \, dx. & \end{array} \right. \tag{4.7}$$

The compatibility constant c_δ is given by

$$c_\delta = \frac{1}{|\Omega|} \left(\int_{\partial\Omega} q^* \, dS - \int_\Omega b_\delta \, dx \right) dx = c - \frac{1}{|\Omega|} \sum_{i=1}^m \alpha_i. \tag{4.8}$$

Now, let us specify the ansätze (4.4) and (4.5) associated with the Case 1. After subtracting problem (3.2) from (4.6) and also (3.3) from (4.7), it follows that v_i and h_i are respectively solutions of the following boundary value problems:

$$\left\{ \begin{array}{rcl} -\Delta v_i &=& \delta_i \quad \text{in} \quad \Omega, \\ v_i &=& 0 \quad \text{on} \quad \partial\Omega, \end{array} \right. \tag{4.9}$$

and

$$\left\{ \begin{array}{rcll} -\Delta h_i &=& \dfrac{1}{|\Omega|} & \text{in} \quad \Omega, \\ -\partial_n h_i &=& \partial_n v_i & \text{on} \quad \partial\Omega, \\ \displaystyle\int_\Omega h_i \, dx &=& 0, & \end{array} \right. \tag{4.10}$$

where $\delta_i(x) := \delta(x - x_i)$. The function v_i is solution of a singular problem with homogeneous boundary condition. On the other hand, the function h_i is solution of a regular problem, since by assumption $x_i \notin \partial\Omega$.

4.2. **Perturbed Problems: Case 2.** Now, let us consider the perturbed counterpart of problems (3.6) and (3.7) associated with partial boundary measurement. They are written as:

$$\left\{ \begin{array}{rcll} -\Delta u_\delta^D &=& b_\delta & \text{in} \quad \Omega, \\ u_\delta^D &=& u^* & \text{on} \quad \Gamma_m, \\ u_\delta^D &=& u^T[b_\delta] & \text{on} \quad \Gamma, \end{array} \right. \tag{4.11}$$

and

$$\left\{ \begin{array}{rcll} -\Delta u_\delta^N &=& b_\delta & \text{in} \quad \Omega, \\ -\partial_n u_\delta^N &=& q^* & \text{on} \quad \Gamma_m, \\ u_\delta^N &=& u^T[b_\delta] & \text{on} \quad \Gamma. \end{array} \right. \tag{4.12}$$

The ansätze (4.4) and (4.5) associated with the Case 2 can now be specified. In fact, let us subtract problem (3.6) from (4.11) and problem (3.7) from (4.12). Then, v_i and h_i are promptly identified as solutions of the following boundary value problems:

$$\left\{ \begin{array}{rcll} -\Delta v_i &=& \delta_i & \text{in} \quad \Omega, \\ v_i &=& 0 & \text{on} \quad \Gamma_m, \\ v_i &=& \displaystyle -\frac{1}{2\pi} \log \|x - x_i\| & \text{on} \quad \Gamma, \end{array} \right. \tag{4.13}$$

and

$$\left\{\begin{array}{rcll} \Delta h_i & = & 0 & \text{in } \Omega, \\ -\partial_n h_i & = & \partial_n v_i & \text{on } \Gamma_m, \\ h_i & = & 0 & \text{on } \Gamma, \end{array}\right. \tag{4.14}$$

where $\delta_i(x) := \delta(x - x_i)$. Note that function v_i is solution of a singular problem, whereas function h_i is solution of a regular problem, since by assumption $x_i \notin \partial\Omega$.

4.3. **Reconstruction Algorithm.** Now, we have all elements to evaluate the difference (4.3) explicitly. In fact, after inserting the ansätze (4.4) and (4.5) in (4.3), we get the following important result:

$$\mathcal{J}(u_\delta^D, u_\delta^N) - \mathcal{J}(u^D, u^N) = -\int_\Omega \left(\sum_{i=1}^m \alpha_i h_i (u^D - u^N)\right) dx + \frac{1}{2}\int_\Omega \left(\sum_{i=1}^m \alpha_i h_i\right)^2 dx \tag{4.15}$$

Note that the expression on the right-hand side of (4.15) depends explicitly on the number m of pointwise sources and their intensities α_i. Moreover, it also depends implicitly on the locations of the pointwise sources x_i through the function h_i, solution of (4.10) or (4.14). Thus, we can define the following function:

$$J(\alpha, \xi, m) := \mathcal{J}(u_\delta^D, u_\delta^N) - \mathcal{J}(u^D, u^N) = -\alpha \cdot d + \frac{1}{2} H\alpha \cdot \alpha \,, \tag{4.16}$$

where $\alpha = (\alpha_1, ..., \alpha_m)$ and $\xi = (x_1, ..., x_m)$. In addition, we observe that the function J is strictly convex with respect to the variable α, so that there exists a global minimum denoted by $\alpha^\star$. In fact, let us minimize $J(\alpha, \xi, m)$ with respect to α, namely:

$$\langle D_\alpha J, \beta \rangle = (H\alpha - d) \cdot \beta = 0, \quad \forall \beta, \tag{4.17}$$

which leads to the following linear system

$$H\alpha = d \,. \tag{4.18}$$

Some terms in the above derivations require explanations. The coefficients of the matrix $H \in \mathbb{R}^{m\times m}$ and the vector $d \in \mathbb{R}^m$ are respectively given by:

$$H_{ki} := A(i,k) = \int_\Omega h_k h_i \, dx \quad \text{and} \quad d_k := b(k) = \int_\Omega h_k (u^D - u^N) \, dx. \tag{4.19}$$

In addition, α solution of (4.18) becomes a function of the locations ξ, namely $\alpha = \alpha(\xi)$. Let us now replace the solution of (4.18) into $J(\alpha, \xi, m)$. Therefore, the optimal locations $\xi^\star$ can be trivially obtained from a combinatorial search over the domain Ω, solution to the following minimization problem

$$\xi^\star = \underset{\xi \in X}{\operatorname{argmin}} \left\{ J(\alpha(\xi), \xi, m) = -\frac{1}{2}\alpha(\xi) \cdot d \right\} \,, \tag{4.20}$$

where X is the set of admissible source locations. Finally, the optimal intensities are given by $\alpha^\star = \alpha(\xi^\star)$. In summary, our method is able to find in one step the optimal intensities $\alpha^\star$ and locations $\xi^\star$ for a given m. The problem on how to find the optimal number of pointwise sources $m^\star$ will be discussed in the numerical experiments section.

In order to summarize the calculations presented in this section we introduce now the resulting reconstruction algorithm. It describes the process of obtaining the optimal parameters $\alpha^\star$ and $\xi^\star$ from the computational point of view. The entries of the algorithm are listed below:

- The quantity m of pointwise sources to be reconstructed;
- The n-points on which the systems (4.18) are solved;
- The vector d and the matrix H whose entries are given by (4.19);

The reconstruction algorithm returns optimal intensities $\alpha^\star$ and locations $\xi^\star$. The reconstruction procedure written in pseudo-code format is shown in Algorithm 1.

Algorithm 1: Reconstruction Algorithm

Data: m, n, d, H
Result: $S^\star$, $\alpha^\star$, $\xi^\star$

Initialization: $S^\star \leftarrow \infty$; $\alpha^\star \leftarrow 0$; $\xi^\star \leftarrow 0$;
for $i_1 \leftarrow 1$ **to** n **do**
  for $i_2 \leftarrow i_1 + 1$ **to** n **do**
    $\vdots$
    for $i_m \leftarrow i_{m-1} + 1$ **to** n **do**

$$d \leftarrow \begin{bmatrix} b(i_1) \\ b(i_2) \\ \vdots \\ b(i_m) \end{bmatrix}; \quad H \leftarrow \begin{bmatrix} A(i_1,i_1) & A(i_1,i_2) & \cdots & A(i_1,i_m) \\ A(i_2,i_1) & A(i_2,i_2) & \cdots & A(i_2,i_m) \\ \vdots & \vdots & \ddots & \vdots \\ A(i_m,i_1) & A(i_m,i_2) & \cdots & A(i_m,i_m) \end{bmatrix};$$

      $I \leftarrow (i_1, i_2, ..., i_m)$; $\xi \leftarrow \Pi(I)$; $\alpha \leftarrow H^{-1}d$; $S \leftarrow -\frac{1}{2} d \cdot \alpha$;
      if $S < S^\star$ **then**
        $\xi^\star \leftarrow \xi$;
        $\alpha^\star \leftarrow \alpha$;
        $S^\star \leftarrow S$;
      end if
    end for
  end for
end for
return $S^\star$, $\alpha^\star$, $\xi^\star$

In the above algorithm Π maps the vector of nodal indices $I = (i_1, i_2, ..., i_m)$ into the corresponding vector of nodal coordinates ξ. As can be noted in the reconstruction Algorithm 1, the optimal solution $(\xi^\star, \alpha^\star)$ is obtained through an exhaustive and combinatorial search over the n-points. Therefore, the complexity $\mathcal{C}(n, m)$ of the algorithm can be evaluated by the formula:

$$\mathcal{C}(n,m) = \left(\begin{array}{c} n \\ m \end{array} \right) m^3 = \frac{n!}{m!(n-m)!} m^3. \tag{4.21}$$

In Fig. 2 the graphics of $m \times \log_{10}(\mathcal{C}(n, m))$ for $n = 100$ and $n = 400$ are presented in blue and red, respectively.

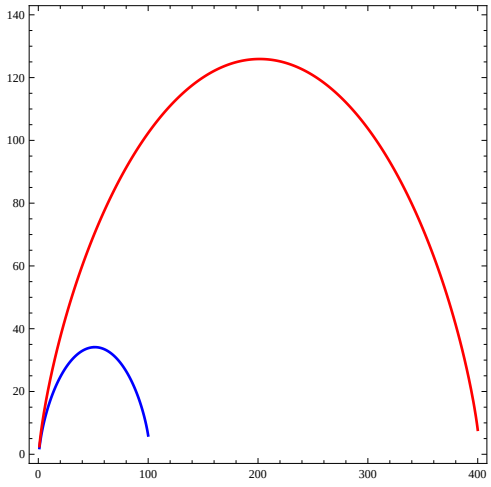

FIGURE 2. Complexity order of Algorithm 1: $m \times \log_{10}(\mathcal{C}(n, m))$, for $n = 100$ in blue and $n = 400$ in red.

Since Algorithm 1 is the bottleneck of the proposed pointwise source reconstruction method, two alternative and more efficient procedures are presented in Appendix A. The first one is based on a multi-grid approach, while the second algorithm is based on a metaheuristic procedure.

5. Numerical results

In this section we present some numerical examples in order to demonstrate the efficiency of the method proposed in this work. In the examples we consider that $\Omega = (-0.5, 0.5) \times (-0.5, 0.5)$ is the hold-all domain and that the initial guess $b \in C_\delta(\Omega)$ is identically zero, that is $b = 0$ in Ω. Moreover, Dirichlet boundary data is imposed on Γ_m using the Newtonian potential (3.5) evaluated in b^*, so that the associated Neumann boundary data q^* corresponds to the boundary measurement on Γ_m. The auxiliary boundary value problems are solved using the Finite Element Method. An initial uniform grid of size 100×100 is generated and each resulting square is divided into four triangles, leading to 4×10^4 finite elements. The functions u^D, u^N, v_i and h_i are computed over this mesh. From these functions the sensitivity of the functional (3.1) with respect to the set of admissible pointwise sources (2.2), given by (4.16), can be numerically evaluated at any point of the mesh. From this mesh a sub-grid is defined where the combinatorial search is performed, leading to the optimal solution $(\alpha^\star, \xi^\star)$ defined in the sub-grid. Each obtained pointwise source is represented by a circle, where the center corresponds to the location while the radius is proportional to the intensity. In the case of noisy data, the boundary measurement q^* is replaced by $q^*_\mu = q^*(1+\mu\eta)$, where η is a function assuming random values in $(-1, 1)$ and μ corresponds to the noise level.

5.1. **Case 1: Total boundary measurement.**

In this section we present three examples concerning total boundary measurement. The first example shows the sensitivity of the reconstruction with respect to the size of the sub-grid. In the second example we propose a procedure to find the unknown number of pointwise sources. In the third example we investigate the robustness of the method with respect to noisy boundary measurement.

5.1.1. *Example 1: Sensitivity of the reconstruction with respect to the size of the sub-grid.* The purpose of this example is to analyse the sensitivity of the reconstruction with respect to the size of the sub-grid. We consider a target given by one pointwise source located at $x^* = (0.14, -0.23)$, with intensity $\alpha^* = 6$. Four uniform sub-grids with 5×5, 20×20, 50×50 and 100×100 nodes are considered. The obtained results for each sub-grid are presented in Table 1, where we observe that the more refined is the sub-grid the better is the reconstruction. When the location x^* belongs to the sub-grid, the reconstruction becomes exact. In the next examples we define a uniform sub-grid of size 20×20 nodes, which represents a good compromise between resolution and computational effort [6]. In order to show different features of the Algorithm 1, we assume from now on that the locations x^* belongs to the sub-grid.

Table 1. Example 1: Results for different sizes of the sub-grid.

Sub-grid	5×5	20×20	50×50	100×100
$\xi^\star$	$(0.10, -0.20)$	$(0.15, -0.25)$	$(0.14, -0.24)$	$(0.14, -0.23)$
$\alpha^\star$	5.0829	5.5307	5.8187	6.0000

5.1.2. *Example 2: Seeking for the number of pointwise sources.* In this example the target consists of three pointwise sources located at $x_1^* = (-0.20, 0.20)$, $x_2^* = (-0.25, -0.25)$, and $x_3^* = (0.15, 0.00)$, with intensities $\alpha_1^* = 1$, $\alpha_2^* = 2$ and $\alpha_3^* = 3$. The representation of the target is shown in Fig. 3. We start the reconstruction algorithm by taking $m = 1$ and proceed to increasing the value of m until that the vector of optimal intensities $\alpha^\star$ contains one entry with negligible value. The results are shown in Fig. 4. For $m = 1$ and $m = 2$ the solutions are clearly far from the target. For $m = 3$ the locations and intensities are perfectly reconstructed. Finally, for $m = 4$ there is an additional pointwise source with negligible intensity, namely $\alpha_4^\star = 1.2342 \times 10^{-12}$. Therefore we can conclude that the correct quantity of pointwise sources is

$m = 3$. Note that this procedure is not iterative, since there is no relation between the results for two consecutive values of m. In addition, we can start the Algorithm 1 based on the assumption that there exists $m > m^*$ and find a number $(m - m^\star)$ of trial balls with negligible sizes in just one shot.

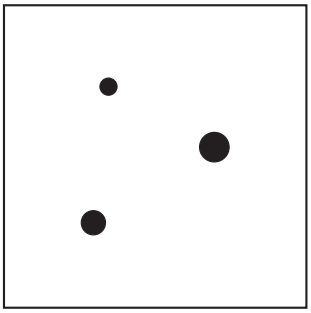

FIGURE 3. Example 2: Target

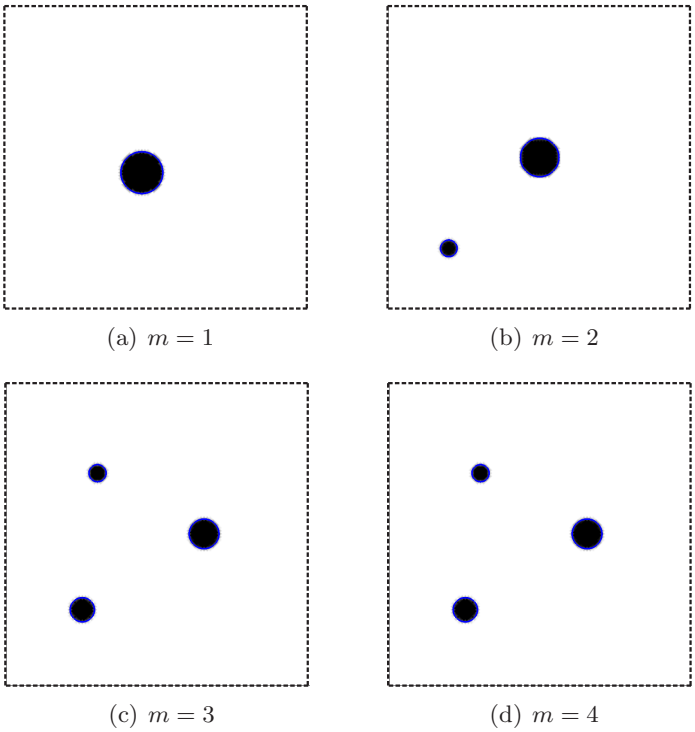

(a) $m = 1$ (b) $m = 2$

(c) $m = 3$ (d) $m = 4$

FIGURE 4. Example 2: Results.

5.1.3. *Example 3: Noisy boundary data.* Now we are interested in investigating the robustness of the method with respect to noisy boundary data. The target contains three pointwise sources located at $x_1^* = (-0.20, 0.20)$, $x_2^* = (-0.25, -0.25)$ and $x_3^* = (0.15, 0.00)$ with same intensities $\alpha_i^* = 4$, $i = 1, 2, 3$. The target representation is shown in Fig. 7. The boundary measurement q^* is corrupted with white Gaussian noise (WGN) of zero mean and different values of standard deviation. The obtained results for standard deviation μ corresponding to 5%, 10%, 20% and 40% of noise are presented in Figs. 6(a), 6(b), 6(c) and 6(d), respectively.

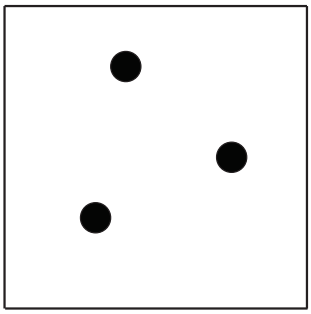

FIGURE 5. Example 3: Target

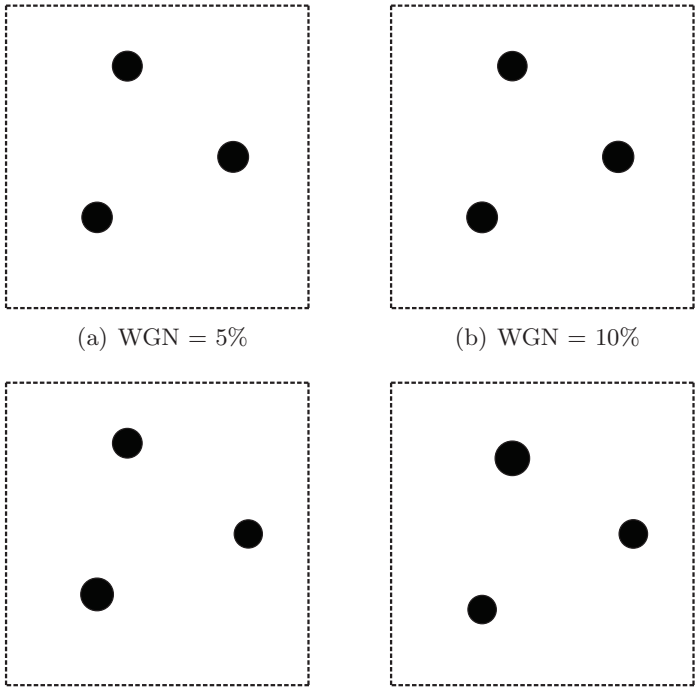

(a) WGN = 5% (b) WGN = 10%

(c) WGN = 20% (d) WGN = 40%

FIGURE 6. Example 3: Results.

5.2. **Case 2: Partial boundary measurement.** In this section we show two examples related to partial boundary measurement. The idea is to investigate the influence of the size of Γ_m in the reconstruction process with and without noise on the boundary measurement.

5.2.1. *Example 4: Without noise.* The target is given by two pointwise sources located at $x_1^* = (0.00, 0.20)$ and $x_2^* = (0.00, -0.20)$ and with intensities $\alpha_1^* = 10$ and $\alpha_2^* = 1$, as can be seen in Fig. 7. The obtained results for different sizes of the set Γ_m are shown in Figs. 8(a), 8(b), 8(c) and 8(d) for $|\Gamma_m| = 1.0$, $|\Gamma_m| = 0.8$, $|\Gamma_m| = 0.4$ and $|\Gamma_m| = 0.1$, respectively. Note that the reconstruction is exact even when Γ_m is considerably small. This fact corroborates with the result demonstrated in [16], where the reconstruction of a star-shaped source is ensured provided that $|\Gamma_m| \neq 0$.

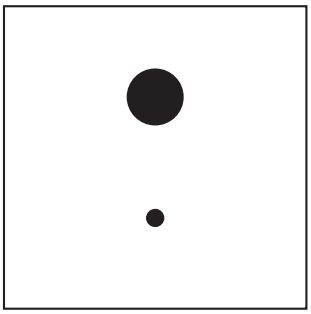

FIGURE 7. Example 4: Target

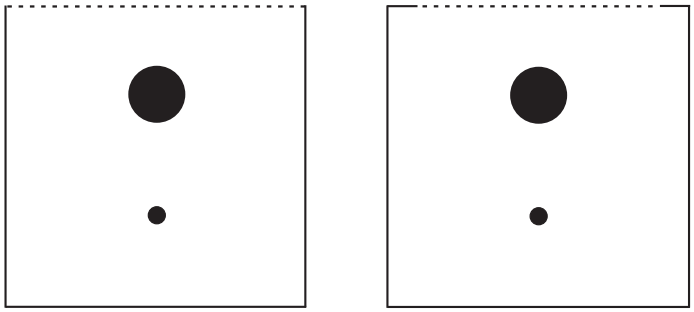

(a) $|\Gamma_m| = 1.0$ (b) $|\Gamma_m| = 0.8$

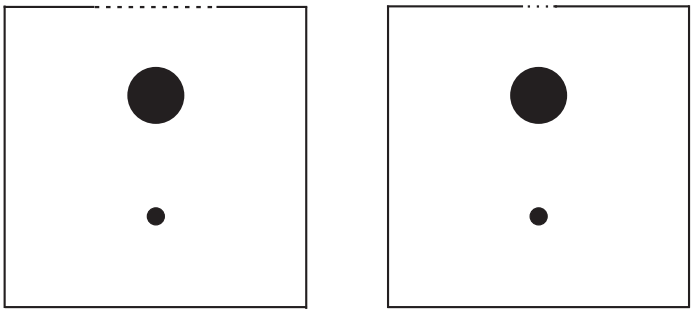

(c) $|\Gamma_m| = 0.4$ (d) $|\Gamma_m| = 0.1$

FIGURE 8. Example 4: Results.

5.2.2. *Example 5: With noise.* In this example the target shown in Fig. 9 is given by two pointwise sources located at $x_1^* = (0.00, 0.20)$ and $x_2^* = (0.00, -0.20)$ and with intensities $\alpha_i^* = 5$, $i = 1, 2$. The boundary measurement q^* is corrupted with white Gaussian noise (WGN) of zero mean and standard deviation μ corresponding to 5% of noise. The obtained results for $|\Gamma_m| = 1.0$, $|\Gamma_m| = 0.8$, $|\Gamma_m| = 0.4$ and $|\Gamma_m| = 0.1$ are presented in Figs. 10(a), 10(b), 10(c) and 10(d), respectively. In contrast to Example 3, here the smaller is Γ_m the worst is the reconstruction.

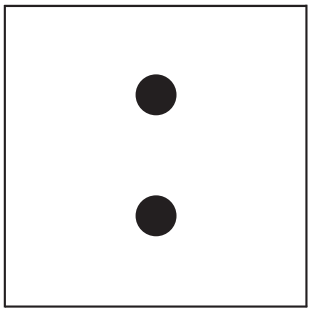

FIGURE 9. Example 5: Target

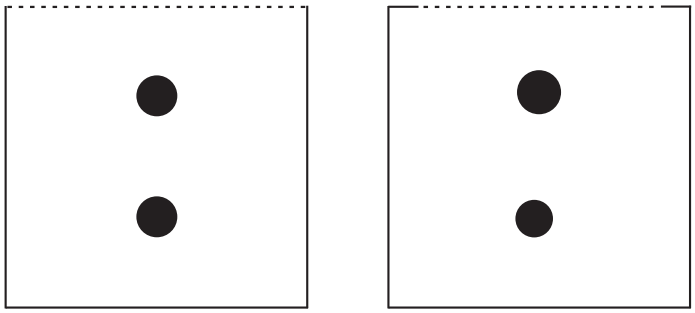

(a) $|\Gamma_m| = 1.0$ (b) $|\Gamma_m| = 0.8$

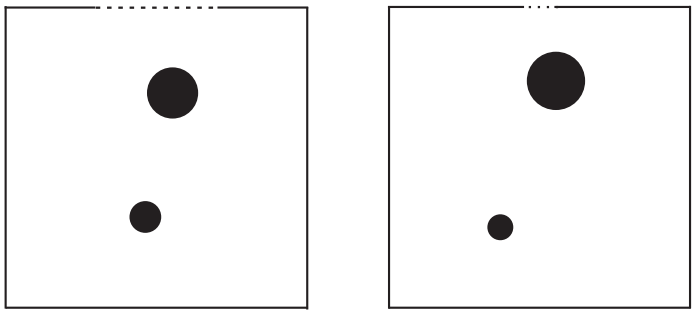

(c) $|\Gamma_m| = 0.4$ (d) $|\Gamma_m| = 0.1$

FIGURE 10. Example 5: Results.

6. Conclusion

In this paper a new method for pointwise sources reconstruction from total or partial boundary measurements has been proposed. The main idea consists in reformulate the inverse problem as an optimization problem, where a Kohn-Vogelius type functional is minimized in the set of admissible pointwise sources. The sensitivity of the Kohn-Vogelius functional with respect to the admissible set of pointwise sources has been explicitly evaluated. From these results, a new non-iterative second-order reconstruction algorithm has been devised. In particular, for a given number of pointwise sources, it returns their optimal intensities and locations. The number of pointwise sources can be find after some trials. In addition, the reconstruction is exact without noise and the algorithm is very robust with respect to noisy data. These features have been shown through some numerical experiments. Finally, two alternative and more efficient reconstruction algorithms are presented in Appendix A.

Acknowledgements

This research was partly supported by CNPq (Brazilian Research Council), CAPES (Brazilian Higher Education Staff Training Agency) and FAPERJ (Research Foundation of the State of Rio de Janeiro). These supports are gratefully acknowledged.

Appendix A. Alternative Reconstruction Algorithms

As described in Section 4.3, the reconstruction Algorithm 1 performs an exhaustive search over the n-points in order to obtain the optimal intensities $\alpha^\star$ and locations $\xi^\star$ for a given number of pointwise sources m. Since we are dealing with a combinatorial problem, such exhaustive search becomes rapidly infeasible for $n \gg m$ as m increases. For example, in trial tests, when using Algorithm 1, the optimal solution cannot be efficiently obtained in the sub-grid with $n = 20 \times 20$, when $4 < m \ll n$. See Fig. 2. Since Algorithm 1 is clearly the bottleneck of the proposed pointwise source reconstruction method, in this appendix two alternative reconstruction algorithms are presented. The first one is based on a multi-grid procedure, while the second algorithm is based on a metaheuristic approach.

A.1. **Multi-grid approach.** After an inspection of Fig. 2, we note that the complexity of Algorithm 1 goes down very quickly when $m \sim n$. Moreover, in Example 1 of Section 5 we observe that when x_i^* does not belong to the sub-grid, the reconstruction algorithm finds the optimal location $x_i^\star$ over the sub-grid, which is closest to the x_i^*. Therefore, we propose a multi-grid approach which takes advantages of these features. The basic idea consists in defining an initial sub-grid G_0 with a number n of nodes, such that $n \sim m$. In this way, the number of combinations becomes small and consequently Algorithm 1 runs very fast. After solving the exhaustive search in G_0, we obtain the vector of optimal locations $\xi_0^\star$ over the sub-grid G_0. The next step consists in refining G_0 in the neighbourhood of $\xi_0^\star$ in order to produce a new sub-grid G_1. The exhaustive search is solved in G_1 and a new vector of optimal locations $\xi_1^\star$ is obtained within the sub-grid G_1. This procedure is then repeated until a desired resolution is attained. See sketch of the multi-grid procedure in Algorithm 2.

Algorithm 2: Multi-grid Reconstruction Algorithm.

Data: m,n,d,H,K

Define the initial sub-grid G_0
Perform the combinatorial search over G_0 *using Algorithm 1*
for $k \leftarrow 1$ **to** K **do**
    Refine previous sub-grid to obtain the new one G_k
    Perform the combinatorial search over G_k *using Algorithm 1*
end for

The parameters m, n, d and H represent the same as in Algorithm 1 and K is the number of refinements necessary to the initial grid reaches the same resolution of the finite element mesh.

Note that the proposed multi-grid procedure becomes iterative, since the solution obtained in the finer sub-grid depends on the previous one. Nevertheless, such an approach allows to deal with a large number of pointwise sources m in a feasible computational cost. This fact is confirmed through some numerical experiments presented in the Section A.3.

A.2. **Metaheuristic approach.** In contrast to the deterministic method presented in Section A.1, here we propose a stochastic approach based on metaheuristic ideas, which is capable of finding good quality solutions in a relatively low computational cost. The proposed *evolutionary algorithm* (EA), largely known as a *metaheuristic*, does not guarantee to find the global optimal solution but a good approximation of it in a reasonable time.

Metaheuristics can be seen as a high level framework which combines basic heuristic methods in order to efficiently explore the search space. In comparison with classical optimization methods, where a single solution is modified at each iteration and the outcome of the method is a single optimized solution, in EAs a population of solutions is modified in each iteration, and

the outcome of the method is also a population of solutions. In the case where the optimization problem has a unique optimum, it is expected that the population members of an EA converge to that optimum solution [11].

Hence, a new algorithm is proposed here for solving the minimization problem described in equation (4.20). This new method is a population based EA which tries to improve a set of solutions by applying *mutation* and *crossover* strategies in each member of the population, followed by two local search procedures which balance *intensification* and *diversification* of the search process. A simplified scheme of the proposed metaheuristic is shown in Algorithm 3.

Algorithm 3: Algorithmic skeleton for the proposed metaheuristic.

```
Data: g_max, Np, ε, T_g, δ, m, n, d, H
Initialize population for g ← 1 to g_max do
    for k ← 1 to Np do
        Performs mutation and crossover
        Apply local search
    end for
    Select the next population
end for
return Best solution
```

The parameters m, n, d and H represent the same as in Algorithm 1. The parameter g_{max} indicates the maximum number of generations, Np is the maximum number of solutions in the population, ϵ and T_g are parameters used in the local search procedure, and $\delta \in [0, 1]$ is the *crossover* probability. Those parameters are user-defined values.

Once initialized, the algorithm performs the search process until g_{max} is reached. At each generation, each solution in the population is mutated and recombined to produce a trial solution, hopefully better than the previous one. After that, local search procedures are applied in order to increase the quality of the trial solutions. Hence, a new population with Np new trial solutions is generated. Those solutions are then compared to the previous ones, and those with better objective function value are selected to constitute the population of the next generation. A detailed description of the components and the steps of the method are presented in the following.

A.2.1. *Structure of candidate solutions.* In the proposed metaheuristic, each solution k in the population, with $k = 1, ..., Np$, is represented by: (i) the m-dimensional vector I_k whose entries are distinct nodal indices belonging to $N = \{1, 2, ..., n\}$; (ii) the n-dimensional vector y_k which contains binary values associated with the indices in I_k; and (iii) the objective function value $F(I_k) := J(\alpha(\Pi(I_k)), \Pi(I_k), m)$ associated with the solution I_k. Table 2 shows an illustrative example of a population of solutions.

TABLE 2. Illustrative example of a population structure with $Np = 5$, $m = 3$ and $n = 6$.

Solution,k	I_k	y_k	$F(I_k)$
1	(2,1,3)	(1,1,1,0,0,0)	-1.53
2	(5,6,4)	(0,0,0,1,1,1)	-2.19
3	(2,4,6)	(0,1,0,1,0,1)	-1.15
4	(6,1,3)	(1,0,1,0,0,1)	-0.69
5	(3,5,4)	(0,0,1,1,1,0)	-2.33

A.2.2. *Initialization.* The algorithm starts with a population of size Np. Each vector I_k is initialized with random distinct indices in the set N, and the binary values are assigned to the associated vector y_k. After that, each solution is evaluated according to the objective function $F(I_k)$.

A.2.3. *Mutation and crossover.* At each generation, the solutions in the population are mutated and recombined to produce an intermediary population of Np mutant solutions. To generate a trial solution I'_k, the mutation process randomly selects two solutions (I_{r_1}, I_{r_2}), in the population and *combine* them to the current solution (I_k), with $r_1 \neq r_2 \neq k$. The mutation strategy is inspired by the *permutation matrix approach* proposed for the differential evolution algorithm when applied to the travelling salesman problem [18]. Hence, two solutions I_{r_1} and I_{r_2} define a *permutation matrix* $\mathcal{P}$ as $y_{r_2} = \mathcal{P}y_{r_1}$. After multiplying $\mathcal{P}$ by the binary vector y_k associated to a third solution I_k, a new trial solution I'_k is obtained. Since all operations are combinations of distinct indices, the resultant trial solutions are always feasible, that is, combinations of distinct indices in the set N. Therefore, for each candidate solution I_k this procedure is performed, where two other solutions I_{r_1} and I_{r_2} are randomly selected to be combined with the current solution I_k. In addition, as suggested in [18], a *crossover* procedure is implemented. The crossover probability $\delta \in [0, 1]$ scales the effect of the permutation matrix $\mathcal{P}$. By setting $\delta = 1$, the permutation matrix is kept unchanged, while with $\delta = 0$ it reduces the permutation matrix to diagonal form. By using intermediate values for $\delta \in (0, 1)$, just a fraction of the permutations defined by $\mathcal{P}$ is performed.

A.2.4. *Local search procedures.* In the proposed method two local search procedures are applied in order to improve the solutions obtained after the mutation and crossover procedures. These two local searches try to balance the *intensification* of the search by exploiting information obtained until the current generation, and the *diversification* of the search by randomly selecting information to be incorporated at the current solution. Hence, the trial solutions are modified into new solutions by changing one of the corresponding solution components.

The *intensification* phase is performed first. Given a trial solution I'_k, one index in the set N that is not in the trial solution is *probabilistically chosen* to substitute one index in that solution. This probabilistic choice relies on the *roulette wheel selection* procedure of genetic algorithms and ant colony optimization methods [14, 12]: in the *probability vector* $p \in \mathbb{R}^n$, each value $p[i]$ determines a slice on a circular roulette wheel. The size of the slice is proportional to the number of times that an index i appears in the best solution of the previous generation. The more an index appears in candidate solutions the greater is the probability that the index is selected to be replaced in the current solution. If the replacement of an index in the trial solution generates an improved solution, then this new solution is considered, otherwise the trial solution is kept unchanged.

Thereafter, the *diversification* phase is performed. Given a trial solution I'_k, possibly modified in the intensification phase, one index in the set N that is not in the trial solution is randomly selected to be replaced in the trial solution. If the replacement of an index generates a better solution, then this new modified solution is considered, otherwise the trial solution is kept unchanged.

The probability vector p is initialized by ϵ, that is, in the first generation all indices in the set N have the same probability to be selected. At the end of each generation, the probability vector p is updated by ϵ only in the assigned indices that appeared in the best solution in the current generation. To avoid stagnation in the selection of the indices, caused by the increase in the value of $p[i]$ associated with indices that appear in the best solution along many generations, the probability vector p is initialized with the initial value ϵ at every T_g generations.

A.3. **Comparative analysis between all approaches.** Let us present a comparative analysis in terms of computational cost between the exhaustive (Algorithm 1), multi-grid (Algorithm 2) and metaheuristic (Algorithm 3) approaches. All algorithms were implemented in Matlab and the experiments were performed in a workstation running Windows 7 with Intel Core i5 and 8 GB RAM. For Algorithms 1 and 3, a sub-grid with 20×20 nodes is defined. For Algorithm 2, three nested sub-grids are defined with 5×5, 10×10 and 20×20 nodes. Therefore, in all cases we have the same final resolution. In the case of Algorithm 3, five independent runs were performed for different values of m with the following parameters setting: $g_{max} = 1500$, $Np = 50$, $\epsilon = 10^{-5}$, $\delta = 0.5$ and $T_g = 200$. Finally, Fig. 11 shows the computational time

from all methods considering different values for pointwise sources m. For the metaheuristic, the average computational time from five runs are presented.

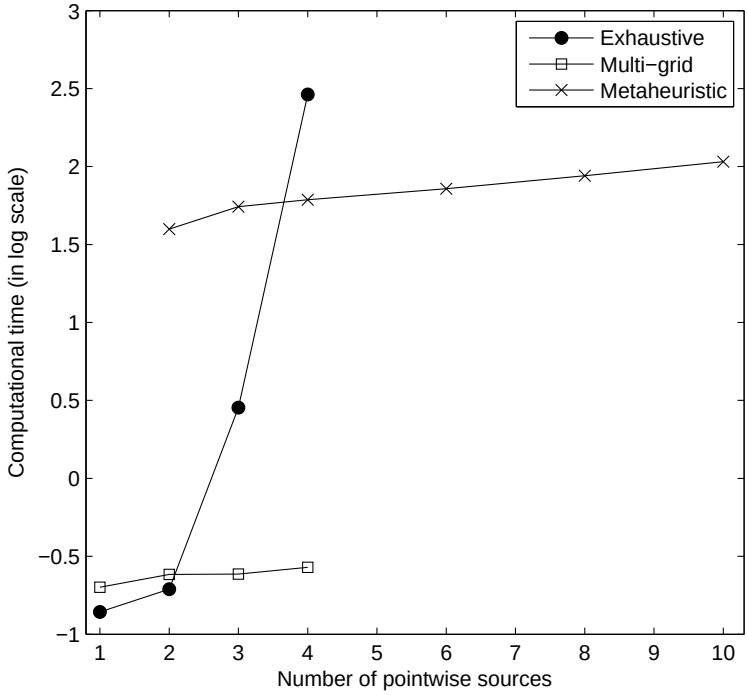

FIGURE 11. Comparison of the computational time of all approaches.

For $m = 4$, the exhaustive method takes 270 seconds while the multi-grid approach takes less than 0.27 seconds, which denotes a decrease of about 1000 times in the computational time. For the metaheuristic, the average computational time in five runs is about 120 seconds for $m \leq 10$. It is possible to observe that the increase of the computational time of both the multi-grid and the metaheuristic approaches is not directly proportional to the increase in the parameter m, which shows stability of these methods regarding the scalability of the problem. Moreover, this fact indicates that the multi-grid is able to reconstruct a large number of sources in a reasonable time.

Regarding the metaheuristic, it is important to highlight that for $m = 2, 3, 4, 6, 8$ the algorithm finds the optimal solution in all executions. For $m = 10$, the optimal solution was found in 20% of the executions. Although in some executions the optimal solution was not found, the final results reported can give an idea about the optimal locations $\xi^\star$ and intensities $\alpha^\star$, since the resulting solutions are close to the optimal one. It is also important to mention that the metaheuristic is capable of reaching the optimal solution using less number of generations than the one used in these experiments, as can be observed in Fig. 12.

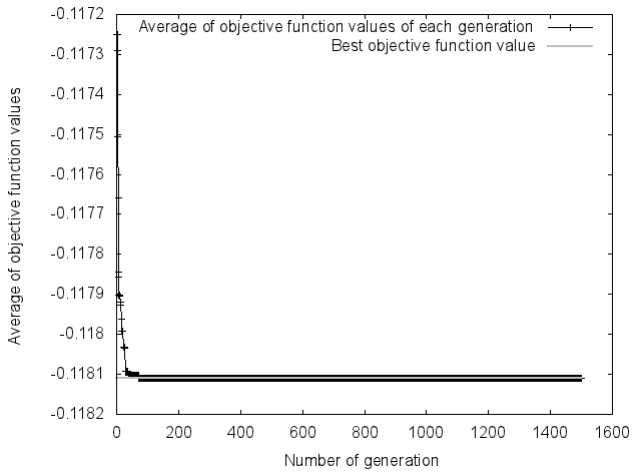

(a) $m = 2$.

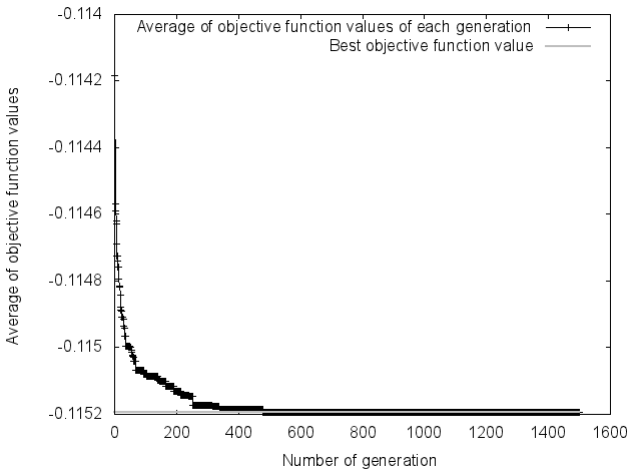

(b) $m = 3$.

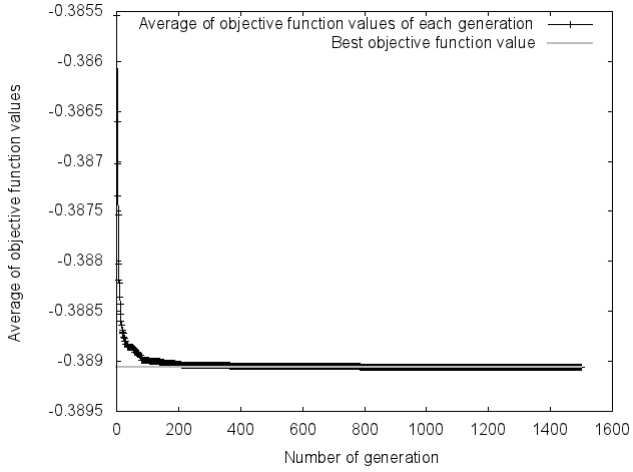

(c) $m = 4$.

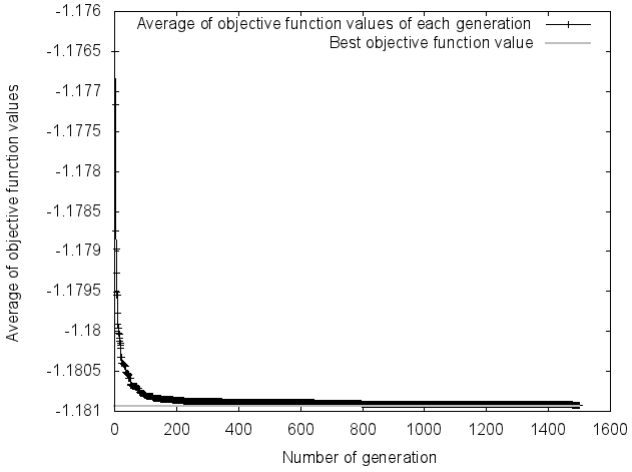

(d) $m = 6$.

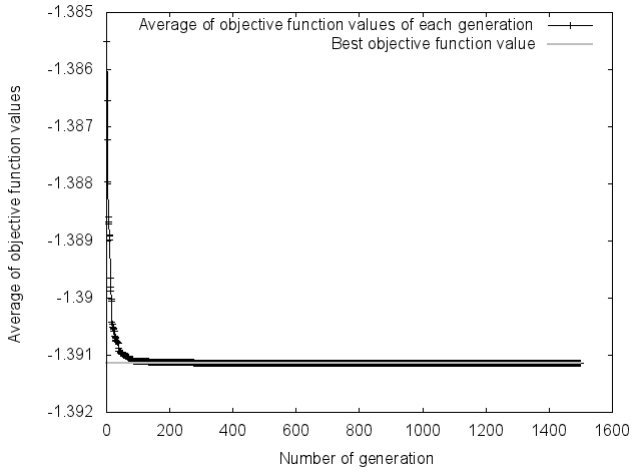

(e) $m = 8$.

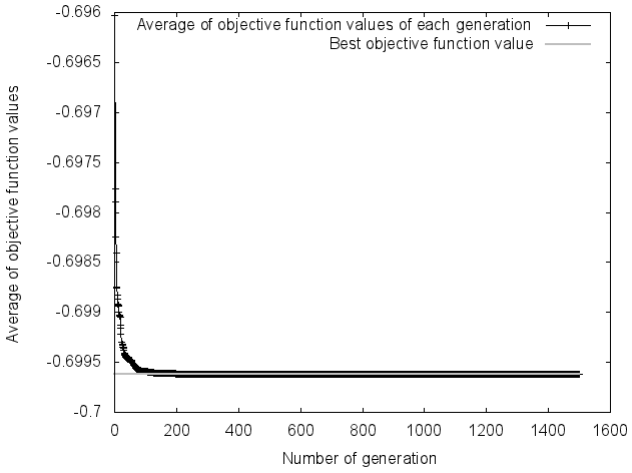

(f) $m = 10$.

FIGURE 12. History of the average of the best objective function value in each generation from five runs.

REFERENCES

[1] H. Ammari and H. Kang. *Reconstruction of small inhomogeneities from boundary measurements.* Lectures Notes in Mathematics vol. 1846. Springer-Verlag, Berlin, 2004.

[2] A. El Badia and T. Ha-Duong. An inverse source problem in potential analysis. *Inverse Problems*, 16:651–663, 2000.
[3] A. El Badia and T. Ha-Duong. On an inverse problem for the heat equation, with application to identifying a pollution source. *Inverse Ill-Posed Problems*, 10:585–599, 2002.
[4] F. Barthelmes and R. Dietrich. Use of point masses on optimized positions for the approximation of the gravity field. In R. H. Rapp and F. Sansò, editors, *Determination of the Geoid*, volume 106 of *International Association of Geodesy Symposia*, pages 484–493. Springer New York, 1991.
[5] G. Buttazzo, N. Varchon, and H. Zoubairi. Optimal measures for elliptic problems. *Annali di Matematica*, 185(2):207–221, 2006.
[6] A. Canelas, A. Laurain, and A. A. Novotny. A new reconstruction method for the inverse potential problem. *Journal of Computational Physics*, 268:417–431, 2014.
[7] A. Canelas, A. Laurain, and A. A. Novotny. A new reconstruction method for the inverse source problem from partial boundary measurements. *Inverse Problems*, 31(7):075009, 2015.
[8] E. Casas and E. Zuazua. Spike controls for elliptic and parabolic PDE. *Systems and Control Letters*, 62(4):311–318, 2013.
[9] D. J. Cedio-Fengya, S. Moskow, and M. S. Vogelius. Identification of conductivity imperfections of small diameter by boundary measurements. Continuous dependence and computational reconstruction. *Inverse Problems*, 14(3):553–595, 1998.
[10] C. Clason and K. Kunisch. A duality-based approach to elliptic control problems in non-reflexive banach spaces. *ESAIM: Control, Optimisation and Calculus of Variations*, 17(1):243–266, 2009.
[11] K. Deb. *Multi-Objective Optimization using Evolutionary Algorithms*. John Wiley & Sons, New York, NY, USA, 2001.
[12] M. Dorigo and T. Stutzle. *Ant Colony Optimization*. The MIT Press, London, England, 2004.
[13] O. Faugeras et al. The inverse EEG and MEG problems: the adjoint space approach. Technical Report No 3673, Institut National de Recherche en Informatique et en Automatique, 1999.
[14] D. E. Goldberg. *Genetic Algorithms in Search, Optimization and Machine Learning*. Addison-Wesley Longman, Boston, USA, 1989.
[15] S. He and V. Romanov. Identification of dipole sources in a bounded domain for maxwell's equations. *Wave Motion*, 28:25–40, 1998.
[16] V. Isakov. *Inverse source problems*. American Mathematical Society, Providence, Rhode Island, 1990.
[17] V. Isakov, S. Leung, and J. Qian. A fast local level set method for inverse gravimetry. *Communications in Computational Physics*, 10(4):1044–1070, 2011.
[18] R. M. Storn K. V. Price and J. A. Lampinen. *Differential Evolution: A Practical Approach to Global Optimization*. Springer-Verlag, 2005, Belin.
[19] R. Kohn and M. Vogelius. Determining conductivity by boundary measurements. *Comm. Pure Appl. Math.*, 37(3):289–298, 1984.
[20] V. Komornik and M. Yamamoto. Upper and lower estimates in determining point sources in a wave equation. *Inverse Problems*, 18(2):319–329, 2002.
[21] A. Leitão and J. Baumeister. *Topics in Inverse Problems*. IMPA Mathematical Publications, Rio de Janeiro, 2005.
[22] K. Pieper and B. Vexler. A priori error analysis for discretization of sparse elliptic optimal control problems in measure space. *SIAM Journal on Control and Optimization*, 51(4):2788–2808, 2013.

Laboratório Nacional de Computação Científica LNCC/MCT, Coordenação de Matemática Aplicada e Computacional, Av. Getúlio Vargas 333, 25651-075 Petrópolis - RJ, Brasil
E-mail address: novotny@lncc.br